Detection and Categorisation of Multilevel High-sensitivity Cardiovascular Biomarkers from Lateral Flow Immunoassay Images via Recurrent Neural Networks

Min Jing[1], Donal McLaughlin[2], David Steele[3], Sara McNamee[1], Brian MacNamee[4], Patrick Cullen[1], Dewar Finlay[1] and James McLaughlin[1]

[1]*Nanotechnology and Integrated BioEngineering Centre (NIBEC), Ulster University, U.K.*

[2]*Department of Physics, University College London, U.K.*

[3]*Biocolor Ltd, U.K.*

[4]*School of Computer Science, University College Dublin, Republic of Ireland*

Keywords: Lateral Flow Immunoassays (LFA) Image, High-sensitivity Cardiovascular Biomarkers, Classification, Long Short-Term Memory (LSTM), Point-of-Care (PoC).

Abstract: Lateral Flow Immunoassays (LFA) have the potential to provide low cost, rapid and highly efficacious Point-of-Care (PoC) diagnostic testing in resource limited settings. Traditional LFA testing is semi-quantitative based on the calibration curve, which faces challenges in the detection of multilevel high-sensitivity biomarkers due its low sensitivity. This paper proposes a novel framework in which the LFA images are acquired from a designed CMOS reader system under controlled lighting. Unlike most existing approaches based on image intensity, the proposed system does not require detection of region of interest (ROI), instead each row of the LFA image was considered as time series signals. The Long Short-Term Memory (LSTM) network was deployed to classify the LFA data obtained from cardiovascular biomarker, C-Reactive Protein (CRP), at eight concentration levels (within the range 0-5mg/L) that are aligned with clinically actionable categories. The performance under different arrangements for input dimension and parameters were evaluated. The preliminary results show that the proposed LSTM outperforms other popular classification methods, which demonstrate the capability of the proposed system to detect high-sensitivity CRP and suggests the potential of applications for early risk assessment of cardiovascular diseases (CVD).

1 INTRODUCTION

Cardiovascular disease (CVD) is considered as a major threat to global health. There is a growing demand for a range of portable, rapid and low cost biosensing devices for the early detection of CVD. Lateral Flow Immunoassays (LFA) are effective Point-of-Care (PoC) devices that have attracted increased attention recently because they can provide low cost, rapid and highly efficacious PoC diagnostic testing in resource limited settings. Although LFA have found widespread applications in POC diagnostics, the low sensitivity of LFA limits their ability to detect biomarkers, such as C-Reactive Protein (CRP), which are normally present in low concentration in blood (Ridker, 2003). CRP is a protein that increases in the blood with inflammation or infection as well as following a heart attack, surgery, or trauma. According to the National Institute of Health and Care Excellence's (NICE) guidelines measuring CRP quantitatively over concentration levels between 10mg/L to 100 mg/L can assess the severity of bacterial infection. High-sensitivity CRP (hs-CRP) tests performed over a lower range (from 0.5mg/L to 10 mg/L) can be used for early risk assessment of cardiovascular diseases (CVD) (Ridker et al., 2000).

Detection of multilevel high sensitivity biomarkers via LFA testing is a challenging task. Studies have been carried out to improve the detection sensitivity to allow the development of high sensitivity assays (Torres and Ridker, 2003), improve the labeling strategies, enhance the optical and electrochemical transducers and explore the evolution of recognition (Mak et al., 2016). Several methods have been developed to enhance the sensitivity of LFA, such as sample concentration (Moghadam et al., 2015), fluidic control (Rivas et al., 2014), temperature–humidity technique (Choi et al., 2016), probe-based signal enhancement (Hu et al., 2013), enzyme-based signal amplification (Hu et al., 2014) and electrochemical devices-based enhancement (Cheung et al., 2015). However, these approaches require either external equipment, high-

Jing, M., McLaughlin, D., Steele, D., McNamee, S., MacNamee, B., Cullen, P., Finlay, D. and McLaughlin, J.
Detection and Categorisation of Multilevel High-sensitivity Cardiovascular Biomarkers from Lateral Flow Immunoassay Images via Recurrent Neural Networks.
DOI: 10.5220/0009117901770183
In *Proceedings of the 13th International Joint Conference on Biomedical Engineering Systems and Technologies (BIOSTEC 2020) - Volume 2: BIOIMAGING*, pages 177-183
ISBN: 978-989-758-398-8; ISSN: 2184-4305

cost reagents, or complicated fabrication with multi-step procedure. To date, a low-cost, convenient and equipment-free sensitivity enhancement method has not been fully explored.

The use of smartphones has been reported for LFA tests recently (Eltzov et al., 2015) (Quesada-González and Merkoçi, 2017). However most of these applications are focused on simple binary classification based on image intensity. In most cases, the LFA image data are obtained from scanners or smartphone cameras, in which the performance can be affected by image quality due to data being acquired under ambient lights. Most smartphone-based LFA testing are based on popular machine learning approaches such as Support Vector Machine (SVM). Very limited studies have attempted to apply neural networks to LFA scenarios with a different focus to this study. For example, Deep Belief Networks (DBN) were applied in (Zeng et al., 2016) to improve the efficiency of ROI detection rather than classification. Multi-Layer Perceptron (MLP) neural network was used in (Carrio et al., 2015) for drugs-of-abuse detection based on average image intensity from the ROI, which assessed saliva content but not blood based biomarkers.

Recurrent Neural Networks (RNN) are a class of artificial neural networks that are capable of exhibiting dynamic behaviour along a temporal sequence. Long Short-Term Memory (LSTM) networks (Hochreiter and Schmidhuber, 1997) are a special kind of RNN that are able to learn long-term dependencies in time series data that have been successfully applied to speech recognition (Fernández et al., 2007), language modelling (Jozefowicz et al., 2016) and ECG arrhythmia detection (Picon et al., 2019) (Xiong et al., 2018). In this study, we explore the potential of applying LSTM to detect multilevel hs-CRP by considering the LFA image data as time series signals.

Most existing approaches are based on the average of image intensity from the LFA test line area, therefore the performance can be affected by the detection of ROI. This study treats the LFA data along the sample flow direction as time series signals therefore no ROI detection is needed. Note that the purpose of this study is not to analyse the LFA strip at discrete or continuous time points as the assay proceeds. Instead the LFA images were captured at a fixed time point (also known as an endpoint assay), following 'completion' of the lateral flow assay. The LFA image is a final snapshot of the assay which contains a particular spatial phenomenon, i.e., the leading edge is stronger than the trailing edge, which also contains valuable time-dependent information. Considering the LFA as time series signals provides a novel perspective to analyse the LFA data and helps to explore richer information than image intensity. This study investigated the dependence of data length, input dimension and hidden layers in LSTM and the results demonstrate the advantages and potential of the proposed framework.

The rest of paper is organised as follows. In Section 2 the structure of LFA is explained and an example of LFA data is presented. In Section 3, the proposed framework is described before the LSTM network is explained, followed by the arrangement of LFA data for the input sequence. The experimental results are given in Section 4 with the conclusion and future work presented subsequently.

2 LFA & IMAGE DATA

A schematic illustration of LFA is given in Figure 1, which shows the sample pad, sample flow direction, conjugate pad, test line (T-line), control line (C-line) and absorbent pad. The conjugate pad, usually colloidal gold, is labelled with antibodies specific to the target analyte. When the sample is placed on the sample pad, it flows by capillary action to the conjugate pad where the target analyte can interact (bind) with these labelled conjugate antibodies. Conjugate and any conjugate-sample complexes then travel laterally along the strip. Upon reaching the T-line, any formed conjugate-sample complexes are captured and may begin to accumulate over the remainder of the assay time. Once these reach sufficient density a visual change occurs on the T-line. The C-line captures any particle so therefore always appears regardless of presence of the target analyte.

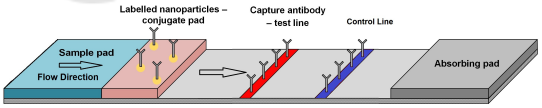

Figure 1: The schematic illustration of the LFA structure.

For traditional devices like an image scanner and smartphone cameras, the image quality can be affected by lighting conditions. In this study a CMOS reader system has been designed in which the LFA image data were acquired from an opaque box under controlled lighting condition. Figure 2 gives examples of LFA strip images obtained at eight hs-CRP concentration levels using the designed CMOS reader system. The eight levels (in mg/L) are: 0, 0.05, 0.1, 0.2, 0.5, 1, 2.5 and 5. It can be seen that each strip contains the C-line and T-line, in which the intensity of the T-line changes according to the concentration

levels. It is also noticed that the position of the T-line varies in each image. For those approaches based on image intensity from the T-line area, the performance is highly dependent on the accurate detection of the T-line area. Features based on image intensity works for simple binary classification but a more sophisticated approach is needed for detection of high sensitivity biomarkers, such as hs-CRP with a concentration level range lower than 5mg/L as outlined in this study.

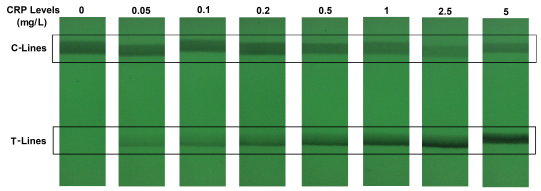

Figure 2: Examples of LFA strip images obtained from eight hs-CRP concentration levels.

3 PROPOSED METHODS

3.1 System Overview

The proposed framework is shown in a block diagram in Figure 3. For the purposes of this study, only the area containing the T-line is needed for testing because the C-line does not reflect the change of concentration level in the sample. In a fully integrated analysis system the formation of the C-line would be used as a quality control check to ensure the assay has performed correctly. Therefore, we directly select the half LFA image containing the T-line without further detection of T-line area. The half LFA image is then divided into a number of mini LFA strips, which are then used as the input sequences for the LSTM network. The total number of input sequences is dependent on the dimension of the mini strips. Once the data has been arranged, they are fed into an LSTM layer followed by a fully connected layer, a softmax layer and an output layer for sequence classification.

3.2 Long Short-Term Memory Network

LSTM is one type of RNN that can learn and remember over long sequences of input data, such as data up to 200 to 400 time steps. Like most neural networks, one benefit of LSTM is that it can learn from the raw time series data directly and therefore does not require feature extraction. In the LSTM, the system updates the information for current state based on the previous state via different gates. A block diagram

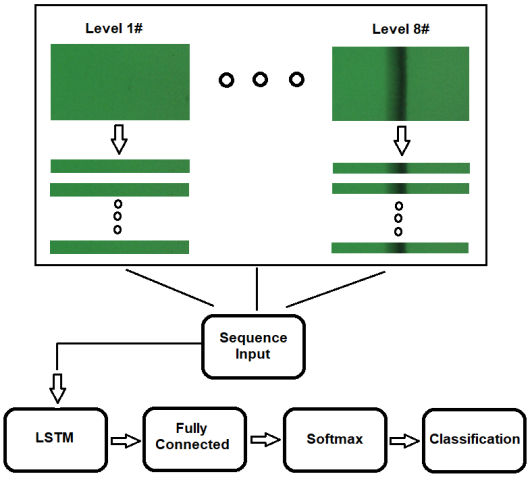

Figure 3: The block diagram for the proposed framework including arrangement of LFA data for LSTM.

of the LSTM is given in Figure 4, which includes the cell state $\mathbf{c}_t$ and the hidden state (output state) $\mathbf{h}_t$ at time t. At each time step t, the LSTM updates the output and cell state by considering the cell state and output at previous time step ($\mathbf{c}_{t-1}$, $\mathbf{h}_{t-1}$). Also seen from Figure 4, there are four components to control the system, i_t, f_t, g_t and o_t, which denote the input gate, forget gate, cell candidate and output gate, respectively.

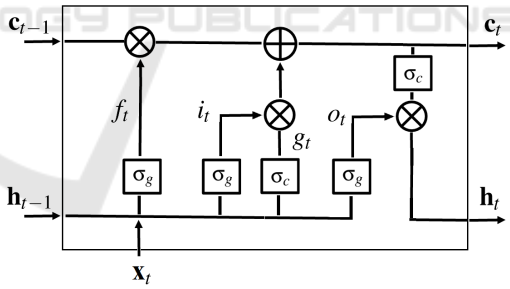

Figure 4: Illustration of LSTM model.

Given a time series sequence $\mathbf{X}$ with k features (channels) of length N, the input sequence for LSTM at the current state t can be presented as a vector $\mathbf{x}(t) = [x_1(t), x_2(t), ..., x_k(t)]^T$ where T denotes the transpose operation. Mathematically, the formulas for the network in forward direction can be presented as (Hochreiter and Schmidhuber, 1997):

$$\mathbf{c}_t = f_t \bigodot \mathbf{c}_{t-1} + i_t \bigodot g_t \quad (1)$$

where $\bigodot$ denotes the Hadamard product (element-wise multiplication of vectors).

$$\mathbf{h}_t = o_t \bigodot \sigma_c(\mathbf{c}_t) \quad (2)$$

where σ_c is the state activation function, which the hyperbolic tangent function (tanh) is used. For each gate, the network is updated by:

$$i_t = \sigma_g(\mathbf{W}_i \mathbf{x}_t + \mathbf{R}_i \mathbf{h}_{t-1} + b_i) \quad (3)$$

$$f_t = \sigma_g(\mathbf{W}_f \mathbf{x}_t + \mathbf{R}_f \mathbf{h}_{t-1} + b_f) \quad (4)$$

$$g_t = \sigma_c(\mathbf{W}_g \mathbf{x}_t + \mathbf{R}_g \mathbf{h}_{t-1} + b_g) \quad (5)$$

$$o_t = \sigma_g(\mathbf{W}_o \mathbf{x}_t + \mathbf{R}_o \mathbf{h}_{t-1} + b_o) \quad (6)$$

where the parameters $\mathbf{W} = [\mathbf{W}_i, \mathbf{W}_f, \mathbf{W}_g, \mathbf{W}_o]^T$, $\mathbf{R} = [\mathbf{R}_i, \mathbf{R}_f, \mathbf{R}_g, \mathbf{R}_o]^T$ and $\mathbf{b} = [b_i, b_f, b_g, b_o]^T$ are the input weights, recurrent weights and bias, respectively.

3.3 Data Preparation for LSTM

As mentioned earlier, only half of the LFA image containing the T-line was used. The image dimension is 450 pixels $\times$ 800 pixels, in which 450 is the width of LFA strip and 800 is the length from left to right across the strip (along the flow direction). We consider each row of images as a time series (with 800 time-steps) as they contain the information that arises as a result of temporo-spatial interactions throughout the assay time (via the gradual accumulation of label conjugate particles).

The sequence input for the LSTM is made by a number of mini LFA strip images, and each sequence can be presented as:

$$\mathbf{X} = \begin{pmatrix} x_{11} & x_{12} & \dots & x_{1N} \\ x_{21} & x_{22} & \dots & x_{2N} \\ \vdots & \vdots & \ddots & \vdots \\ x_{k1} & x_{k2} & \dots & x_{kN} \end{pmatrix} \quad (7)$$

Here the length of time steps N is defined by the length of the LFA strip which is 800. The dimension k is determined by the width of the mini strip, which may vary depending how the experiment is designed. Therefore, the total number of input sequences is dependent on the dimension (width) of the mini strips, which is $450/k$. The dependence between the dimension of mini strips and the number of sequences was investigated by changing the width from 10 pixels to 90 pixels. The performances were evaluated and the results are presented in Section 4.4.

4 EXPERIMENTS & RESULTS

4.1 Setup

This study contains the LFA data obtained based on eight hs-CRP concentration levels. For each level (class), we have 30 LFA images in total. Note the number of images is not the number of data samples used for the network training and testing because we treat each row of the LFA image as one time series signal. As described in the method section, one LFA image contains 450 time series, so the total number of time series for each class is $450 \times 30 = 13500$ and total number of time series signals available for eight classes is 108,000. The number of input sequences is dependent on the dimension of the mini strips.

For all experiments, a holdout data partition was used, in which 90% (27 images) were randomly selected for training and the remaining 10% (3 images) for testing. The accuracy was defined as: sum (Predict = Test)/(number of Test). The number of epochs, batch size and iteration rate was empirically set to 30, 32 and 0.001 respectively. All numerical aspects of experimentation were conducted using MATLAB2019a.

4.2 Preprocessing

To reduce the high-frequency noise, the LFA time series were first smoothed by moving average via sliding window method. Different window lengths, 2, 5 and 10 were tested in the experiment described in Section 4.3. All data were normalised by z-score to remove the mean value and set variance to unit. An example of normalised LFA time series from eight hs-CRP levels is given in Figure 5, in which the moving window length is 5 and the time steps were down sampled from 800 to 200. The y-axis gives the normalised intensity and the x-axis is the time steps. It can be observed that the signal contains a 'time element' that arises from the interplay between biomarker and label as it develops over time, which provides valuable time-dependent information. Such information is usually ignored in the approaches based on averaging the image intensity within T-line area.

4.3 Dependence with Data Length

To examine the impact of data length on the performance, different data lengths were tested by down sampling the original data (length of 800) to 400 and 200. The input dimension was 45 and the hidden layer for the LSTM was 150 (based on results from Section 4.4). The performances based on different data length and filter length were evaluated and the results are shown in Figure 6. It appears that for filter window length 2, time steps of 400 works better than others. For other cases, a data length of 800 performs better than the other two, however, it takes a much longer time for training compared to the shorter data length.

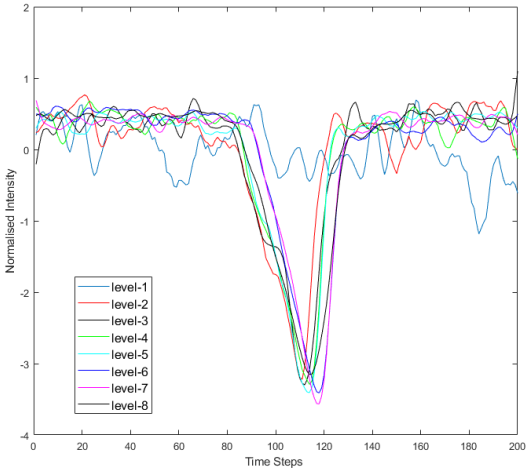

Figure 5: Examples of the normalised LFA time series data obtained at eight hs-CRP concentration levels.

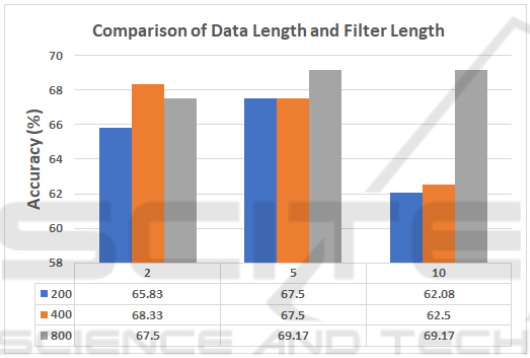

Figure 6: Comparison of results based on different data length and filter window length.

4.4 Dependence with Input Dimension

It was found from the initial testing that the performance can be affected by different settings for the dimension of the mini strips and the number of hidden layers. Therefore, we evaluated the performance by changing these parameters. The dimension of the mini strip were set as 10, 15, 30, 45 and 90. The number of input sequences for the LSTM network is dependent on the dimension of the strip. For example, when we treat the mini strip with a dimension 45 as one sequence, then each LFA strip image can be considered to have 10 sequences. Therefore the total data for training set is 10 (sequences) $\times$ 8 (classes) $\times$ 27 (images) = 2160 and the data size for testing is 10 $\times$ 8 $\times$ 3 = 240. The number of data samples used for training and testing under different input arrangement are given in Table 1. To reduce training time, a data length of 200 and filter length of 5 were used. The performances based on alternative settings are shown in Figure 7, from which it can be seen that the best performance is achieved when the input dimension is 45 and number of hidden layers is 150.

Table 1: Data size based on different input dimension.

(Dimension, Sequences)	Training	Testing
(10, 45)	9720	1080
(15, 30)	6480	720
(30, 15)	3240	360
(45, 10)	2160	240
(90, 5)	1080	120

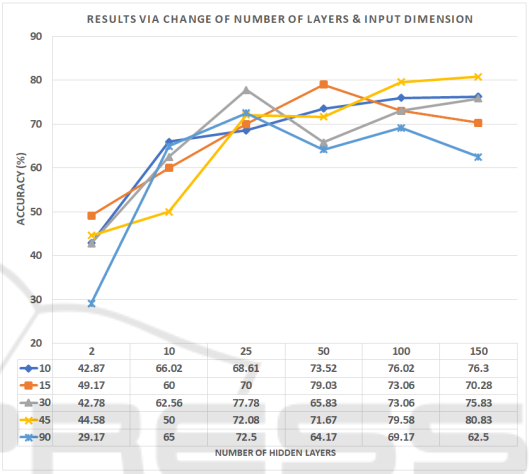

Figure 7: Comparison of results based on different input dimension and number of hidden layers.

4.5 Results for Classification

The performance of the LSTM for classification was compared to six classifiers including SVM, K Nearest Neighbours (KNN), Linear Discriminant Analysis (LDA), Decision Tree (DT), Naive Bayes (NB) and Ensemble. The evaluation was based on different arrangements for input dimensions as shown in Table 1. For fair comparison the same data (partition) was used to test all algorithms. For LSTM, the data length was 200 and filter length was 5. The number of hidden layers was selected based on the best performance from the results in Section 4.4. Since the focus of this study was to investigate the proposed method based on LSTM, the default settings in MATLAB were used for other classifiers, such as for Ensemble, the adaptive boosting was used for multiclass classification. For KNN the number of neighbours was determined based on testing the number of neighbours in a range of 2-8 and the one that gave the best performance was selected.

The comparison of performance for classification based on different input dimension and number of

sequences are promising as seen from the Table 2, which shows that the LSTM outperforms the other methods in all cases. An example confusion matrix based on the LSTM (dimension 45, sequence 10) is given in Figure 8. An example of the Receiver Operating Characteristic (ROC) curve based on the performance from all algorithms is given in Figure 9, which shows that the LSTM performs better than other classification algorithms. The performances for all methods can be improved, such as by fine tuning parameters via cross validation, or including a third independent dataset to chose the optimal number of neighbours in KNN, which will be considered in the next stage of this work.

Table 2: Comparison of Performance for Classification.

	Accuracy (%)				
Classifiers	(10,45)	(15,30)	(30,15)	(45,10)	(90,5)
SVM	49.35	38.61	58.61	43.33	44.17
KNN	53.43	42.36	49.17	37.92	39.17
LDA	52.50	39.31	53.33	39.58	49.17
DT	54.07	47.92	50.28	45.00	43.33
NB	66.20	58.33	62.60	60.42	57.50
Ensemble	56.30	55.83	65.83	55.42	54.17
LSTM	76.30	73.30	73.33	78.75	76.67

5 DISCUSSION

Over the last decade, many biosensors have been developed to detect and quantify cardiac biomarkers in medical diagnostics, in which the signals can be electrochemical, optical, mass change (piezoelectric / acoustic wave) or magnetic in nature (Qureshi et al., 2012). Some of there techniques are relatively demanding in terms of sample preparation, costs, analysis times, and skill levels. In contrast, immunoassays are effective alternatives for rapid screening of samples, such as the enzyme-linked immunosorbent assay (ELISA) and LFA. Main advantages of ELISA are the possibility to analyse multiple samples simultaneously, sensitivity and the relative simplicity. However, ELISA testing is more time consuming than LFA due to the operations like repeated incubation, washing steps and enzyme reaction for final signal generation (Fojtíková et al., 2018). The outcomes from this study are promising which show the improvement of detection of low concentration biomarkers by LFA using proposed LSTM networks. For the future work, a cross-validation can be considered in training to find the optimum parameters for the networks. Techniques based on the time series analysis or image processing can be explored for feature extraction before applying the network, which will potentially improve the performance.

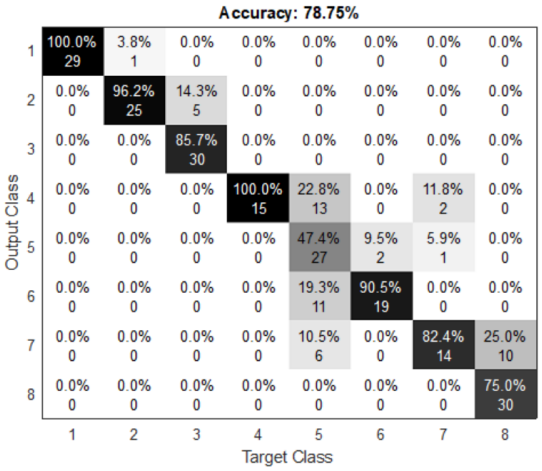

Figure 8: Confusion matrix for classification of eight hs-CRP concentration levels using LSTM.

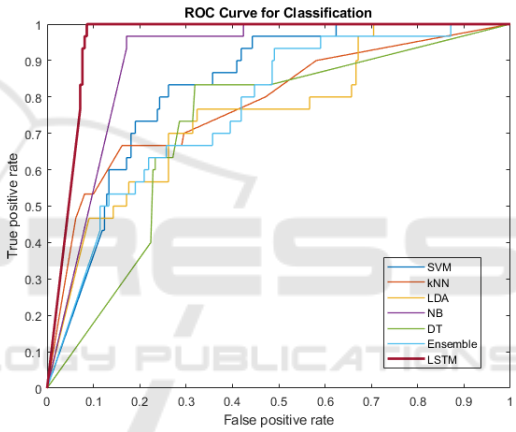

Figure 9: Comparison of ROC curve for classification.

6 CONCLUSIONS

In this study, a novel method for detection of multi-level high-sensitivity CRP biomarkers via LFA testing using LSTM recurrent neural networks is presented. The proposed methods were evaluated using eight hs-CRP levels below 5mg/L which is the CRP range for early risk assessment of CVD. The LFA strip images were collected from a designed CMOS reader system under controlled lighting. Each row of an LFA image is considered as a time series which can be fed to an LSTM model for classification. The dependence between data length, filter window length, input dimension and hidden layers were investigated. The results show that the proposed LSTM approach achieves better performance than other popular machine learning algorithms although the performance can be further improved in future work. The preliminary outcomes

are encouraging and suggest the potential of applying the proposed method for early risk assessment for CVD.

ACKNOWLEDGEMENTS

This research is carried out under the project of Eastern Corridor Medical Engineering Centre (ECME) and funded by the European Unions INTERREG VA Programme, managed by the Special EU Programmes Body (SEUPB).

REFERENCES

Carrio, A., Sampedro, C., Sanchez-Lopez, J., Pimienta, M., and Campoy, P. (2015). Automated low-cost smartphone-based lateral flow saliva test reader for drugs-of-abuse detection. *Sensors*, 15(11):29569–29593.

Cheung, S. F., Cheng, S. K., and Kamei, D. T. (2015). based systems for point-of-care biosensing. *Journal of laboratory automation*, 20(4):316–333.

Choi, J. R., Hu, J., Feng, S., Abas, W. A. B. W., Pingguan-Murphy, B., and Xu, F. (2016). Sensitive biomolecule detection in lateral flow assay with a portable temperature–humidity control device. *Biosensors and Bioelectronics*, 79:98–107.

Eltzov, E., Guttel, S., Low Yuen Kei, A., Sinawang, P. D., Ionescu, R. E., and Marks, R. S. (2015). Lateral flow immunoassays–from paper strip to smartphone technology. *Electroanalysis*, 27(9):2116–2130.

Fernández, S., Graves, A., and Schmidhuber, J. (2007). An application of recurrent neural networks to discriminative keyword spotting. In *International Conference on Artificial Neural Networks*, pages 220–229. Springer.

Fojtíková, L., Šuláková, A., Blažková, M., Holubová, B., Kuchař, M., Mikšátková, P., Lapčík, O., and Fukal, L. (2018). Lateral flow immunoassay and enzyme linked immunosorbent assay as effective immunomethods for the detection of synthetic cannabinoid jwh-200 based on the newly synthesized hapten. *Toxicology reports*, 5:65–75.

Hochreiter, S. and Schmidhuber, J. (1997). Long short-term memory. *Neural computation*, 9(8):1735–1780.

Hu, J., Wang, L., Li, F., Han, Y. L., Lin, M., Lu, T. J., and Xu, F. (2013). Oligonucleotide-linked gold nanoparticle aggregates for enhanced sensitivity in lateral flow assays. *Lab on a Chip*, 13(22):4352–4357.

Hu, J., Wang, S., Wang, L., Li, F., Pingguan-Murphy, B., Lu, T. J., and Xu, F. (2014). Advances in paper-based point-of-care diagnostics. *Biosensors and Bioelectronics*, 54:585–597.

Jozefowicz, R., Vinyals, O., Schuster, M., Shazeer, N., and Wu, Y. (2016). Exploring the limits of language modeling. *arXiv preprint arXiv:1602.02410*.

Mak, W. C., Beni, V., and Turner, A. P. (2016). Lateral-flow technology: From visual to instrumental. *TrAC Trends in Analytical Chemistry*, 79:297–305.

Moghadam, B. Y., Connelly, K. T., and Posner, J. D. (2015). Two orders of magnitude improvement in detection limit of lateral flow assays using isotachophoresis. *Analytical chemistry*, 87(2):1009–1017.

Picon, A., Irusta, U., Álvarez-Gila, A., Aramendi, E., Alonso-Atienza, F., Figuera, C., Ayala, U., Garrote, E., Wik, L., Kramer-Johansen, J., et al. (2019). Mixed convolutional and long short-term memory network for the detection of lethal ventricular arrhythmia. *PloS one*, 14(5):e0216756.

Quesada-González, D. and Merkoçi, A. (2017). Mobile phone-based biosensing: An emerging "diagnostic and communication" technology. *Biosensors and Bioelectronics*, 92:549–562.

Qureshi, A., Gurbuz, Y., and Niazi, J. H. (2012). Biosensors for cardiac biomarkers detection: A review. *Sensors and Actuators B: Chemical*, 171:62–76.

Ridker, P. M. (2003). Clinical application of c-reactive protein for cardiovascular disease detection and prevention. *Circulation*, 107(3):363–369.

Ridker, P. M., Hennekens, C. H., Buring, J. E., and Rifai, N. (2000). C-reactive protein and other markers of inflammation in the prediction of cardiovascular disease in women. *New England Journal of Medicine*, 342(12):836–843.

Rivas, L., Medina-Sánchez, M., de la Escosura-Muñiz, A., and Merkoçi, A. (2014). Improving sensitivity of gold nanoparticle-based lateral flow assays by using wax-printed pillars as delay barriers of microfluidics. *Lab on a Chip*, 14(22):4406–4414.

Torres, J. L. and Ridker, P. M. (2003). High sensitivity c-reactive protein in clinical practice. *American Heart Hospital Journal*, 1(3):207–211.

Xiong, Z., Nash, M. P., Cheng, E., Fedorov, V. V., Stiles, M. K., and Zhao, J. (2018). Ecg signal classification for the detection of cardiac arrhythmias using a convolutional recurrent neural network. *Physiological measurement*, 39(9):094006.

Zeng, N., Wang, Z., Zhang, H., Liu, W., and Alsaadi, F. E. (2016). Deep belief networks for quantitative analysis of a gold immunochromatographic strip. *Cognitive Computation*, 8(4):684–692.